

Finite element simulation of fluid flow in fractured rock media

R. Kristinof · P. G. Ranjith · S. K. Choi

Received: 21 December 2008 / Accepted: 17 June 2009 / Published online: 11 July 2009
© Springer-Verlag 2009

Abstract Fluid dynamics models are used by the petroleum industry to model single- and/or multi-phase flow within fractured rock formations, in order to facilitate extraction of fluids such as oil and natural gas, and in other areas of engineering to study groundwater flow, as well as to estimate contaminant seepage and transport. In this paper, the numerical modelling software *Comsol* is used to simulate air and water flow through a specimen of granite with a single vertical fracture subjected to triaxial loading conditions. The intent of the model is to simulate triaxial test findings on a rock specimen with a natural fracture. Fluid flow is simulated at various confining and inlet pressures using the cubic law. Model results were in good agreement with laboratory findings. Pressure distribution along the fracture and across the specimen are as expected with a near linear pressure distribution along the length of the fracture. A drawdown effect on pressure distribution across the specimen in the vicinity of the fracture is also observed. Pressure gradient was largely uniform; however, some localised zones of high gradient along the fracture are observed.

Keywords Fluid flow · Fractured · Rock · Modelling · Rock joint

Introduction

Many industries, including mining and petroleum, throughout the world rely on the use of fluid dynamics models of reservoirs within fractured rock formations, in order to facilitate extraction of fluids such as oil and natural gas, and for studying groundwater flow, as well as to estimate contaminant seepage and transport. Early work by Witherspoon et al. (1980) and Noorishad et al. (1982) observed that, as a function of confining stress, fluid displacement across the fracture was highly non-linear. Further, the flow was observed to be proportional to a power function of ‘apparent hydraulic aperture’. The exponent of this power law was determined by Witherspoon et al. (1980) to be approximately three, and thus showed that there was a cubic law relationship between fracture aperture and flow rate.

This work was challenged, however, by Pyrak-Nolte et al. (1987) who studied the relationships between mechanical deformation, permeability and void geometry in samples of quartz monzonite rock, which contained a natural fracture. Pyrak-Nolte et al. (1987) observed a very small hysteresis in strain measurements, indicating that even at an effective stress of 85 MPa, deformations were largely elastic. Deformation continued to increase with increasing load, indicating that even at high confining stresses, pore spaces within the fracture were still opened, and thus fluid could still flow. Measurements of flow indicated a sharp drop in flow rate with increasing confining stress, up to a load of approximately 20 MPa. Studies of the metal casts of the fracture walls indicate that this decrease in flow resulted from increase in contact area between fracture walls. Beyond the 20 MPa confining stress, fluid flow plateaued in two of the samples, and in the third continued to decrease (up to the maximum applied

R. Kristinof · P. G. Ranjith (✉)
Department of Civil Engineering, Monash University,
Melbourne, VIC 3800, Australia
e-mail: ranjith.pg@eng.monash.edu.au

S. K. Choi
CSIRO Petroleum, Clayton, Australia

confining stress of 85 MPa), albeit at an extremely low rate of change. This “small but finite” flow indicated that deformation resulting from these high confining pressures are the result of void closure in the rock matrix rather than closure of the fracture itself. Importantly, the trend line of the data in a log–log plot of displacement versus flow rate did not have the slope of 1 in 3 as would be suggested by a cubic law model; rather, the data trended as a general power law, with the exponent varying with confining stress. The investigation by Pyrak-Nolte et al. (1987), however, showed that the cubic law only held in the case of smooth fractures or where the fracture walls ‘register almost exactly’. This was consistent with the type of fracture induced by Witherspoon et al. (1980). In the case of a natural fracture which may be somewhat sheared or irregular, the cubic law does not hold. Hence, it is important to study other flow models. Nevertheless, the cubic law is still an important tool to study fluid flow in simple cases.

Much work has been done on numerical modelling of fluid flow through rock fractures. Zhang and Sanderson (2002) developed a series of 2D numerical models using universal distinct element code (UDEC), a form of discrete element (DE) method. On a macro scale, Zhang and Sanderson (2002) studied flow along fractured zones and faults under varying earth stresses. Several different analyses were performed, including the modelling of hydraulic flow through a non-stationary shear zone, irregular faults and extensional fractures. The effect of dilation of the fault zone due to fluid flow through it was also investigated. Zhang and Sanderson (2002) showed that the numerical technique and code were adequate to simulate these phenomena. They observed that fault slip and associated shearing of rock joints can have an appreciable effect on fluctuations in fluid pressure within the rock, and thus cause irregularities in fluid flow.

Sarkar (2002) recently performed a study into numerical simulation of fluid flow in fractured reservoirs. Unlike previous studies so far cited, the mathematics of this model is based on the Navier–Stokes equation, coupled with the continuity equation. The model developed by assuming fluid-flow velocities would be small enough to ignore inertial terms, which markedly simplifies the calculations. Further, “non-slip” boundary conditions were assigned to flow along the fracture walls meaning that any fluid in contact with the walls will be at rest (Sarkar 2002). This important assumption will be relevant to the Navier–Stokes model used in this project, as boundary conditions will be largely identical. In general, Sarkar (2002) showed that the aperture of the inlet had a greater influence on flow velocity and mass flux than did the outlet aperture. Also, perhaps unsurprisingly, flow was observed to favour wider flow channels than narrower ones. Where multiple flow

channels existed, even where the pressure gradient was the same, the actual mass flux of fluid was greater through a wider channel than through narrower ones. Where a single flow channel branched off into various fractures, the greater flux flowed through the fractures with greater aperture. Even though the permeability of the models investigated were all relatively large (due to the simple geometries), Sarkar (2002) did indicate that permeability is dependent on the relative ‘ease’ of the flow path. Pyrak-Nolte et al. (1987) also suggested that tortuosity was an important factor which affects flow through a fracture. This is intuitive in the sense that one can expect that flow through a highly variable flow path would be less than through a uniform one.

Another study of fluid flow using Navier–Stokes’ equation was undertaken by Zimmerman et al. (2004). This study was used to investigate how much improvement could be obtained using Forcheimer’s modification to Darcy’s law. Zimmerman et al. (2004) showed that flow through the fracture varied from the Darcy (cubic law) model by a factor proportional to the cube of the flow rate, consistent with Forcheimer’s law. This was shown to be relatively insignificant, however (for engineering applications), if the flow velocities were sufficiently small and Reynolds’s numbers were less than 10. Moreover, the Zimmerman model, like Sarkar (2002), showed how the use of the Navier–Stokes equations can be more reliable in a ‘natural’ fracture model than simpler linear models. In general, experimental and numerical results compared well, and showed that transmissivity and flow are consistent with the Forcheimer predictions (as opposed to the simpler Darcy’s law). Generally high precision and low scatter was obtained, with large amounts of scatter only evident at low flow rates, which are attributed to limits of accuracy more than anything else.

Darcy’s law for fluid flow through porous media adequately describes the nature of the flow regime through the rock matrix itself, and through an adaptation known as the cubic law, adequately describes flow through an idealised ‘parallel plate’ void. The applicability of Darcy’s law, however, to more realistic flow regimes, such as flow through a natural fracture is less well-understood (Miskimins and Lopez-Hernandez 2005; Ranjith et al. 2006; Li and Sato 2004). It is hoped that by developing this understanding further through numerical simulation, models can be developed which may ultimately be adapted for use by industry. Using the *Comsol Multiphysics* software package a numerical computer model will be developed to facilitate this investigation. The model will be calibrated against experimental findings, and used to simulate single phase water and air flow through a fractured rock specimen.

Theory: Darcy's law for single phase flow

Darcy's law for fluid flow relates flow rate to pressure gradient via a constant of proportionality k , known as intrinsic permeability. Darcy's law, neglecting the effect of gravity, is expressed in a general form in Eq. 1

$$q = \frac{k}{\mu} A \nabla P. \quad (1)$$

In the above form of the equation, q is in units of m^3/s , μ (dynamic viscosity) in units of Pa s , ∇P is pressure gradient, and A is the cross sectional area of flow (m^2). Intrinsic permeability has the units of m^2 . Darcy's law as expressed here adequately describes the flow regime of viscous fluids through a porous medium; however, for the purposes of modelling fluid flow through a more discrete flow path a different form of equation must be used. Equation 2 is known as Richard's equation, or more commonly as the 'cubic law' for flow through fractures (Miskimins and Lopez-Hernandez 2005).

$$q = \frac{e^3 w}{12\mu} \nabla P \quad (2)$$

In the above flow equation, e is the aperture of the fracture (m), and w the width of the fracture (m). By inspection it can be seen that this equation is equivalent to the general form of Darcy's law, with intrinsic permeability equal to $e^2/12$. This law adequately describes most single phase fluid flows, including water, air and oil, provided viscosities and densities of the fluids are known, and the dimensions of the fracture (flow path) can be ascertained. In naturally occurring situations where fractures are highly irregular, the "hydraulic mean aperture" of the fracture is often used instead of the mechanical aperture, as this may vary greatly along the length of the fracture. Darcy's law assumes that flow is laminar (Zimmerman et al. 2004; Miskimins and Lopez-Hernandez 2005).

Laboratory testing programme

Fractured granite specimens having a diameter of 55 mm and length twice the diameter with low matrix permeability (about 10^{-19} m^2) were selected for the laboratory investigation. The 55-mm diameter core that was used for testing contained a single fracture.

The orientation of the fracture in the triaxial specimen was near vertical. Oil was used as confining fluid in the cell and the axial stress was supplied by a servo-controlled Instron Machine. This is shown in Fig. 1. The magnitude of fluid pressure for each phase and confining pressure were recorded by individual pressure transducers. For a given confining pressure and axial stress, the specimen was first



Fig. 1 Laboratory testing apparatus

saturated with one fluid phase. Individual steady state air flow rates and water flow volumes were recorded by the film flow metre and electronic weighing scale, respectively. Detailed test procedure is given in Ranjith et al. (2006)

Numerical model

Initial model setup

The numerical model used for this analysis was developed using the computer software package *Comsol Multiphysics* 3.2 developed and marketed by ComsolTM. This package allows the development of physical models with varying mathematical complexity. Comsol is packaged with a large number of common physical equations and laws built-in, and also includes a scripting tool to allow new equations to be entered.

The model for this project was built in *Comsol* using standard tools and equations built in to the package. The model was set up using two modules of the software: "Darcy's law—Pressure Analysis—Steady State" (part of the Earth Science Module), and "Plane Stress—Static Analysis" (part of the Structural Mechanics Module). Using the two modules allows a coupled analysis to be performed, which allows the model to compute the interaction between the in situ stresses and the fluid flow. This is important as the in situ stresses change the effective aperture of the fracture, and thus has an obvious influence on the flow regime. Figure 2 shows part of the finite element mesh used in the model. Due to the scale of the model it is difficult to show clearly the geometry of the fracture. For this reason, only a section of the fracture is shown. The actual coordinates of the fracture (assuming origin at bottom left corner of the model) are shown in Table 1. The table identifies the position of the left and right walls of the fracture, respectively, at several vertical ("y") positions.

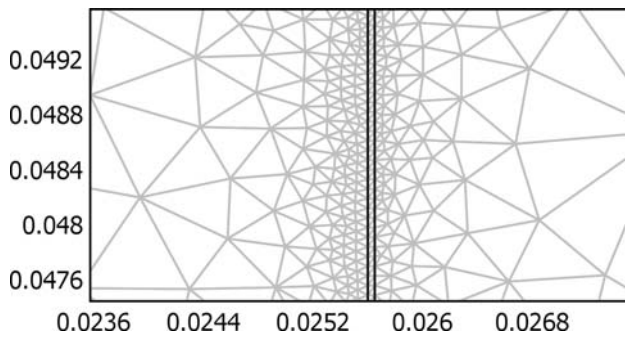


Fig. 2 Geometry of *Comsol* model showing mesh and close up of part of the fracture

Table 1 Fracture Coordinates

Y	Top	Bottom
0	0.0255	0.025515
0.005	0.0256	0.02562
0.01	0.0256	0.025612
0.015	0.0255	0.025533
0.02	0.0256	0.02563
0.025	0.0257	0.02574
0.03	0.0255	0.025521
0.035	0.0255	0.02553
0.04	0.0256	0.02564
0.045	0.0256	0.025651
0.05	0.0256	0.02565
0.055	0.0256	0.025652
0.06	0.0255	0.025563
0.065	0.0255	0.02556
0.07	0.0255	0.025542
0.075	0.0255	0.02557
0.08	0.0255	0.02557
0.085	0.0256	0.025671
0.09	0.0256	0.025652
0.095	0.0256	0.02564
0.1	0.0256	0.025644
0.105	0.0255	0.02553
0.11	0.0256	0.025642

Y position (in metres) along the fracture, *top* vertical coordinate (top of fracture), *bottom* vertical coordinate (bottom of fracture)

The model was solved using the inbuilt stationary non-linear solver, utilising a geometric multigrid linear solver in the predictor step for the initial linear estimation.

Boundary conditions

Boundary conditions are an integral part of the successful development of this numerical model. Using the coupled Darcy's law and Plane Stress models in *Comsol*, boundary conditions have been specified for both flow and triaxial

confining pressure. Flow boundary conditions were specified at the base and at the top of the simulated rock core and were specified in terms of pressure. "inlet pressure", that is, the pressure at which the flow is being propelled was applied along the base of the model, and "atmospheric/gauge pressure" applied along the top. All other boundaries and surfaces were assumed to be no-flow boundaries and were treated as such.

"Cell pressure", equivalent to the triaxial confining pressure applied in the original experiment was applied on all external boundaries. Additionally, a vertical load was applied on the top boundary to simulate the deviatoric stress from the original experiment.

Finite element mesh

Figure 2 shows part of the finite element mesh generated by *Comsol*. A coarse mesh was used for the rock matrix, and an extra fine mesh for the fracture itself. The reason for this is that we are primarily interested in the fluid behaviour within the fracture itself. The permeability of the rock matrix is extremely low (for tested samples), and thus any matrix flow is virtually negligible. As such, the use of a coarse mesh in this part of the model helps to conserve memory and computing power for the more important calculations.

In modelling the flow regime via the Darcy law module of *Comsol*, the key fluid parameters to be entered into the model were density and viscosity, as well as permeability of the fracture and surrounding rock matrix. For the Plane Stress module, strength and stiffness parameters, including Young's modulus and Poisson's ratio of granite were used. Average values for fluid density and viscosity for air and water were used and are shown in Table 2. The granite rock matrix was assigned a permeability of 10^{-19} m^2 , which was considered realistic. It is also sufficiently low to restrict flow through the matrix to a level which would have no noticeable effect on the experimental results.

Modelling of fracture permeability

The permeability of the fracture was the most complicated aspect of the actual model as it is dependent on the properties of the fluid flow, the geometry of the fracture itself, and the influence of both inlet pressure (of the fluid) and

Table 2 Fluid properties used in model

	Water	Air
Viscosity μ (Pa s)	0.001	1.82×10^{-5}
Density ρ (kg/m^3)	1000	1.2

the stresses applied to the rock sample. Several attempts were made to find a single numerical value for the permeability to each fluid; however, failing this, an alternative approach was adopted. From the theoretical discussion of Darcy’s law, the permeability of the fracture is a function of aperture. Equation 3 shows how Darcy’s equation can be rearranged to express aperture as the dependent variable. Adopting the notion of “hydraulic mean aperture”, this equation can then be used to find the average aperture width of the fracture. The permeability (k) of the fracture is given by Eq. 4.

$$e = \left(\frac{12\mu q}{w\nabla P} \right)^{\frac{1}{3}} \tag{3}$$

$$k = \frac{e^2}{12} \tag{4}$$

Data from the experiment were available for the purposes of calibrating this model. For each flow given, the mean hydraulic aperture and thus the permeability of the fracture was determined. A total of 40 data values were available for both water and air single-phase flow. These data points were inspected by both visual and statistical means to determine an empirical relationship between aperture (and thus permeability) and both inlet pressure and triaxial cell pressure. Equations 5 and 6 show the empirical relationships developed for water and air, respectively. The equation for fracture permeability to water was found to have an R^2 value of 95%, and that of air was found to be 82%.

$$e = 1.48358 \times 10^{-4} - 9.112 \times 10^{-6} \ln(P_c) - 6.162 \times 10^{-6} \ln(P_i) \tag{5}$$

$$e = 1.0927 \times 10^{-4} - 1.011 \times 10^{-5} \ln(P_c) - 1.964 \times 10^{-6} \ln(P_i) \tag{6}$$

where P_c = cell pressure (kPa), P_i = inlet pressure (kPa).

From Eqs. 5 and 6 it is apparent that the aperture can be expressed in a general form as in Eq. 7, where a , b and c are functions of fluid properties, joint/fracture roughness, flow pattern through the joint, and whether or not flow can be assumed continuous or discontinuous. Further development of expressions for these constants may be scope for further studies.

$$e = a - b \ln(P_c) - c \ln(P_i) \tag{7}$$

Figures 3, 4, 5 and 6 show the trends in aperture with respect to the two pressure types. It can be seen in Fig. 4 that a similar trend of aperture variation was obtained for all cell pressures. An explanation of this is given in “Single-phase air”. Following the calculation of the above parameters, the model can be run at various cell and inlet pressures, and results obtained. Whilst various types of post

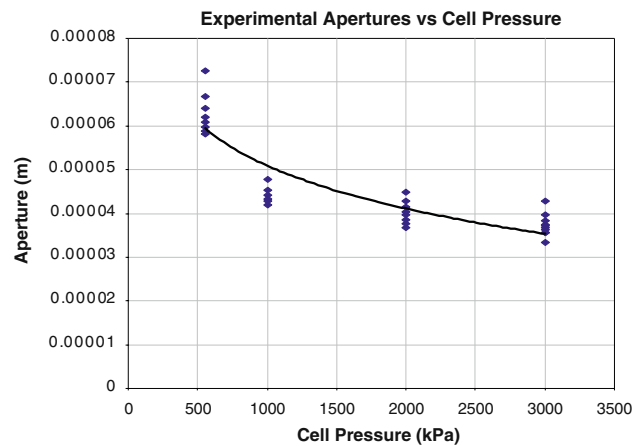


Fig. 3 Experimental apertures versus cell pressure for water flow

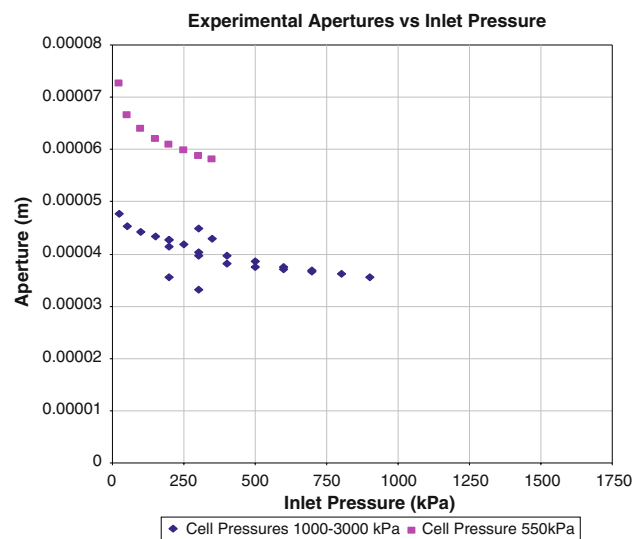


Fig. 4 Experimental apertures versus inlet pressure for water flow

processing data can be produced, for the purposes of this project, only numerical values of fluid velocity are considered necessary. Other parameters will be used as a visual check of the integrity of the model and include pressure distribution and deformation. Velocity can be determined at various intervals along the fracture length, and an average value obtained for the whole fracture. Some consideration was given to using the velocity at the fracture outlet; however, average velocity was considered more appropriate than outlet velocity as it is consistent with the notion of using “average mean aperture” along the fracture length. Equation 8 shows how flow rate can be obtained from this average velocity.

$$q = (v \times 10^6)ew \tag{8}$$

where q has units of ml/s and v (velocity) m/s.

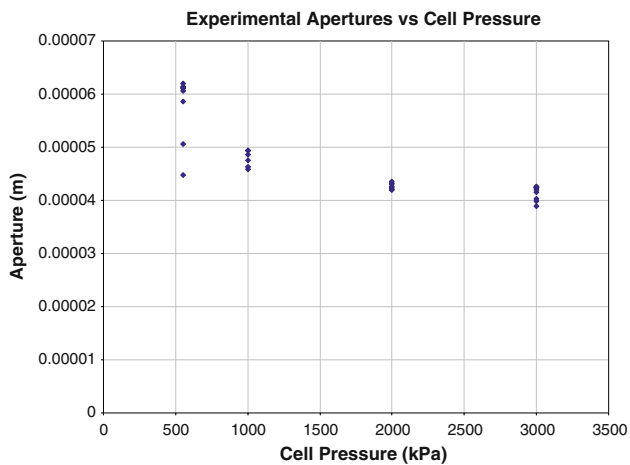


Fig. 5 Experimental apertures versus cell pressure for air flow

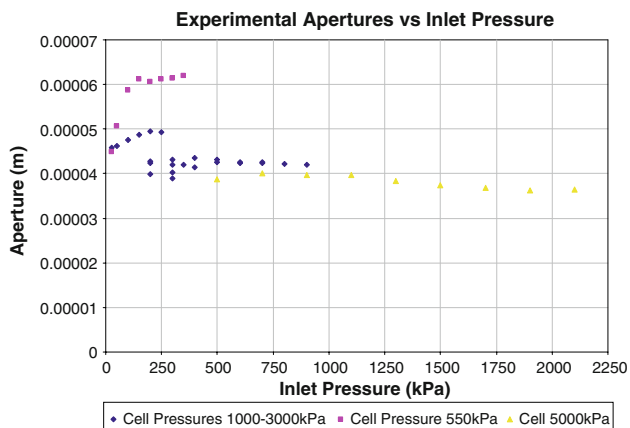


Fig. 6 Experimental apertures versus inlet pressure for air flow

Results and discussion

Single-phase (water)

Figure 7 below shows the relationship between the hydraulic mean apertures as determined by the *Comsol* model (using Eq. 5) and the experimental results obtained from the original experiment. It can be seen that there is reasonable agreement between the two variables, with errors less than 11% in most instances. Given that the model calculates the permeability of the fracture from this aperture value (by Eq. 4), it can be expected that the error in permeability will be less than 23%. This is in fact exactly what is observed.

As can be seen from the above data, there is considerable scatter in the errors obtained. This randomness in the errors suggests that there is no systematic error in the model, which goes some way to validate the methodology

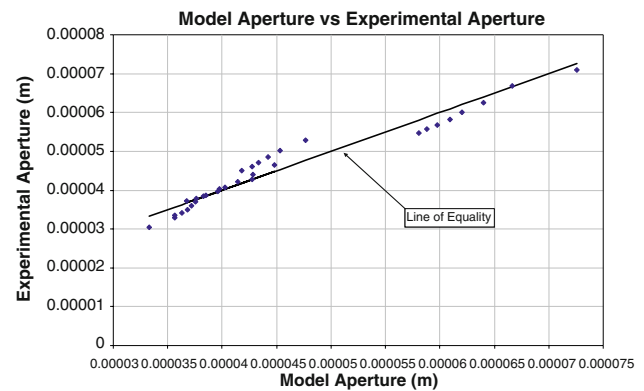


Fig. 7 Model aperture versus experimental aperture for single-phase water flow

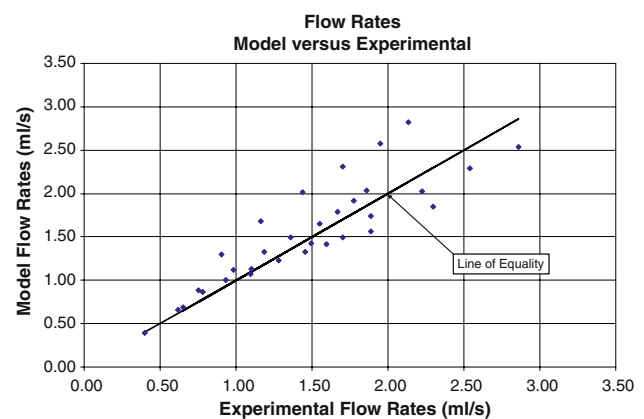


Fig. 8 Model flow rate versus experimental flow rate for single-phase water flow

used. The magnitude of the errors is consistent with the errors implicit in the model, i.e., the errors which result from using Eqs. 3 and 4, which are used in the model to determine velocity. The largest of the errors, apparent at 1,000 kPa cell pressure correspond with the largest errors in aperture. Similarly, much smaller errors correspond to very small aperture errors of 1–4%. The width of the fracture may also be erroneous, as it is assumed to be 55 mm, implying that the fracture is located at the centre of the cylindrical rock sample. Whilst the fracture in the original experiment is located near the centre, it is likely that it was not exactly centred. Finally, the possibility of errors in the experimental results must not be discounted, as this experimental error may also contribute to the discrepancies observed in the simulation.

Figure 8 shows the model and experimental flow rates. Clearly there is a considerable scatter in this data, particularly at high flow rates. The greatest errors result at a cell pressure of 1,000 kPa where the errors are as large as 30% of the experimental flow rate.

Single-phase (air)

Figure 9 shows the relationship between the mean apertures as determined by the *Comsol* model (using Eq. 6) and the experimental results obtained from the original experiment, for the single phase flow of air through the rock fracture. It can be seen that there is a reasonably good agreement between the two variables albeit not as good as was observed with water flow. Errors less than 16% in magnitude are observed.

Again, there appears to be no systematic error in the model as errors are, by inspection, relatively random. The magnitudes of errors in this model are relatively large, and as much as 30% in some cases. Again, larger errors in the above results correspond to larger errors in modelling the aperture of the joint; smaller errors are consistent with smaller aperture errors. One must also include the assumption that the fluid is incompressible. A constant density and viscosity has been assumed for the air flow; however, being a gas it is highly compressible; the model could have underestimated the actual flow velocity, and as

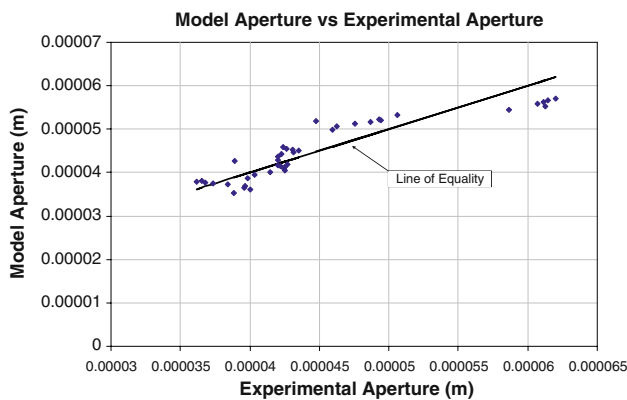


Fig. 9 Model aperture versus experimental aperture for single-phase air flow

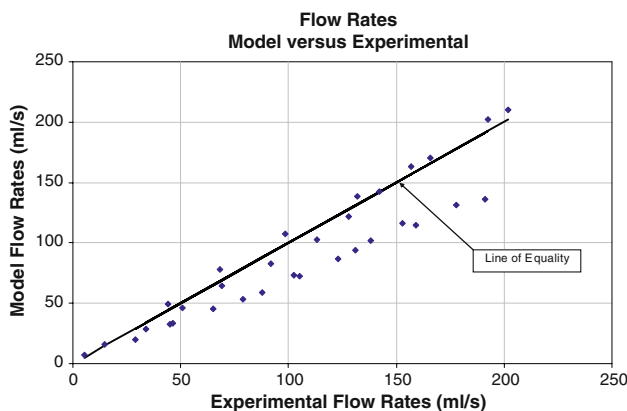


Fig. 10 Model versus experimental flow rates for single-phase air flow

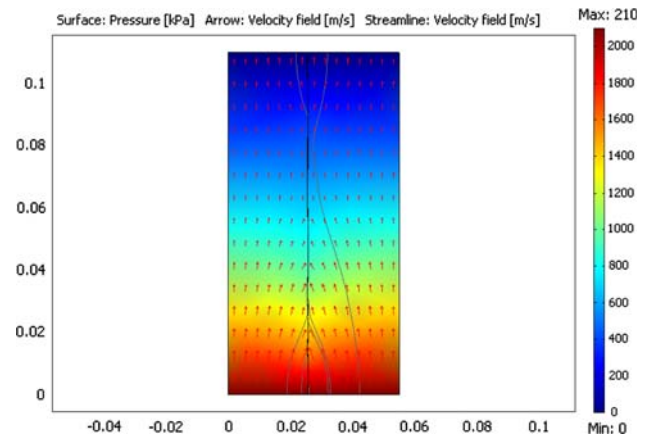


Fig. 11 Pressure distribution and velocity vectors

a result, might give a slight over-estimation of the aperture. Further numerical studies will be carried out to study the influence of changing gas properties within the joint.

Figure 10 shows a plot of the experimental flow rates versus the flows modelled in *Comsol*. As already mentioned, the agreement between the model and the experiment is generally not as good as for water, with many more values having an error greater than 20%. Interestingly though, the magnitude of the largest errors is actually less than that observed for water (25 vs. 30%).

Pressure distribution along the joint

Figures 11, 12 and 13 show various plots of the fluid pressure generated within the specimen. Figure 11 shows a sample output from the model for 2,100 kPa inlet pressure case. It shows pressure distribution across the surface of the model, as well as vectors showing fluid velocity. It should be noted that the size of the velocity vectors are somewhat deceptive. The large arrows suggest that fluid velocity is relatively high through the rock matrix itself; however, it is not due to the scale of the model. It is difficult to see the flow vectors within the fracture itself; however, they are noticeably larger, implying higher velocities, which is naturally the case. Overall this plot shows a pressure distribution throughout the rock sample which is inline with expectations.

Figure 12 shows the pressure distribution along the length of the fracture. The pressure distribution is as expected; however, it is not perfectly linear because of irregularities in the fracture geometry.

Figure 13 shows the pressure distribution along a cross section of the specimen. It is interesting to note that though the pressure distribution is relatively even, there is a noticeable dip in pressure within the fracture, compared to the rock matrix. This is because of the much higher permeability of the fracture compared to the rock matrix. Data

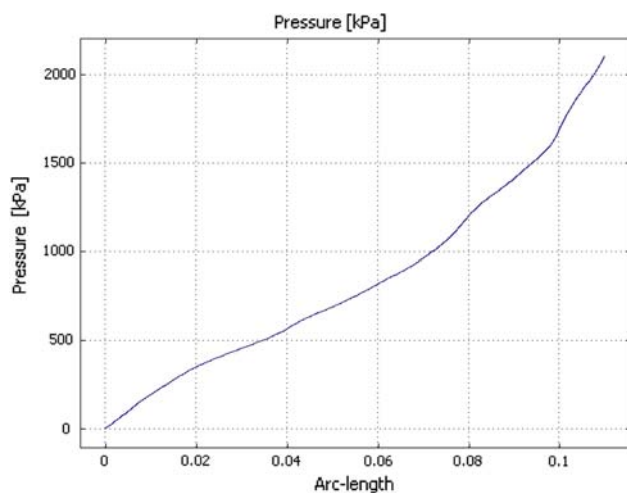


Fig. 12 Pressure distribution along fracture (water flow: 500 kPa cell pressure, 2,100 kPa inlet pressure)

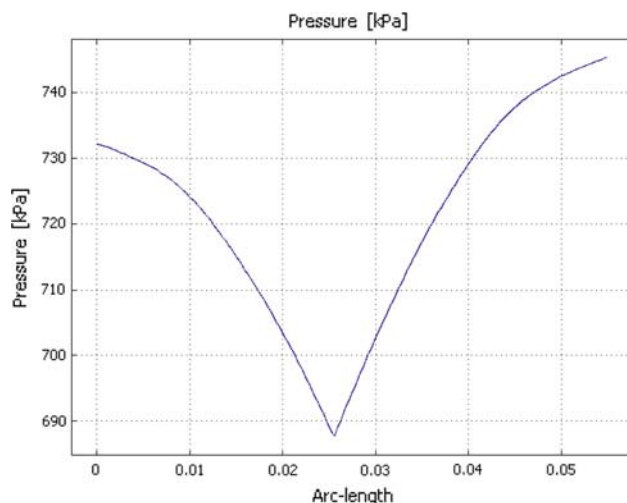


Fig. 13 Pressure distribution across specimen (water flow: 500 kPa cell pressure, 2,100 kPa inlet pressure)

such as that presented in Figs. 11, 12 and 13 is of limited value in an analysis sense; however, it is an extremely useful tool to assist in visualising the problem at hand, and also as a ‘sanity check’, to ensure that the model behaves as expected.

Figure 14 shows a surface plot of the specimen, showing the magnitude of fluid pressure gradients throughout the model. It is interesting to note that though the gradients are relatively uniform in nature, there are localised zones of high gradient around some parts of the fracture. These parts of the fracture are generally narrower than other parts, or more variable in geometry. The figure shows the pressure gradient distribution from the model of water flow; however, the result is the same with air, indicating that it is not affected by fluid properties.

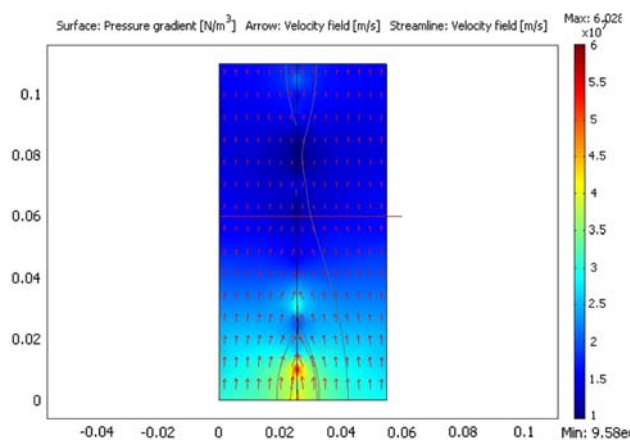


Fig. 14 Pressure gradient plot (water flow: 500 kPa cell pressure, 2,100 kPa inlet pressure)

Conclusion

Single-phase flow through a fractured granite specimen subjected to triaxial loading conditions was examined. Using Darcy’s law and the results from a similar laboratory experiment, a numerical model of a granite specimen with a single vertical fracture was developed. Water and air were allowed to flow through the specimen, under various confining and fluid inlet pressures. The relationship between aperture and confining and inlet pressures was determined. This relationship was found to be logarithmic with respect to both confining and cell pressure, with empirical constants dependent on the properties of the fluid itself.

Results from the model generally show a good satisfactory agreement with the experimental results. Simulation of water flow resulted in errors around 10% of experimental values. Air flow results were also satisfactory, albeit less so than water errors. Investigation of pressure distribution through the model indicated that it behaved as expected, with a near linear pressure variation along the length of the fracture, and a slight drawdown effect across the specimen in the vicinity of the fracture. This is thought to be due to the higher permeability of the fracture with respect to the rock matrix, and the natural tendency of flow towards higher permeability regions. Pressure gradient was observed to be relatively uniform across the specimen; however, localised zones of steep gradient were observed where the fracture geometry was more irregular or narrowed.

References

- Li H, Sato M (2004) Development of a 3D FEM simulator for coalbed two-phase flow with sorption/diffusion. *Int J Rock Mech Min Sci* 41

- Miskimins JL, Lopez-Hernandez HD (2005) Non-Darcy flow in hydraulic fractures: does it really matter? Society of Petroleum Engineers
- Noorishad J, Ayatollahi MS, Witherspoon PA (1982) A finite-element method for coupled stress and fluid flow analysis in fractured rock masses. *Int J Rock Mech Min Sci* 19:185–193. doi: [10.1016/0148-9062\(82\)90888-9](https://doi.org/10.1016/0148-9062(82)90888-9)
- Pyrak-Nolte L, Myer L, Cook NGW, Witherspoon PA (1987) Hydraulic and mechanical properties of natural fractures in low permeability rock. In: Proceedings of International Society for Rock Mechanics. AA Balkema, Rotterdam, pp 225–231
- Ranjith PG, Choi SK, Fourar M (2006) Characterization of two-phase flow in a single rock joint. *Int J Rock Mech Min Sci* 43:216–223
- Sarkar S (2002) Fluid flow simulation in fractured reservoirs. Earth Resources Laboratory, Massachusetts Institute of Technology, Cambridge
- Witherspoon P, Wang J, Iwai K, Gale JE (1980) Validity of cubic law for fluid flow in a deformable rock fracture. *Water Resour Res* 16:1016–1024
- Zhang X, Sanderson DS (2002) Numerical analysis of fluid flow and deformation in fractured rock masses. Pergamon, Oxford
- Zimmerman RW, Al-Yarrubi A, Pain CC, Grattoni CA (2004) Non-linear regimes of fluid flow in rock fractures. *Int J Rock Mech Min Sci* 41(3)